Developing Algorithm for Operational GOES-R Land Surface Temperature Product

Yunyue Yu, Dan Tarpley, Jeffrey L. Privette, Mitchell D. Goldberg, M. K. Rama Varma Raja, Konstantin Y. Vinnikov, and Hui Xu

***Abstract*—The Geostationary Operational Environmental Satellite (GOES) program is developing the Advanced Baseline Imager (ABI), a new generation sensor to be carried onboard the GEOS-R satellite (launch expected in 2014). Compared to the current GOES Imager, ABI will have significant advantages for retrieving land surface temperature (LST) as well as providing qualitative and quantitative data for a wide range of applications. The infrared bands of the ABI sensor are designed to achieve a spatial resolution of 2 km at nadir and a noise equivalent temperature of 0.1 K. These improve the imager specifications and compare well with those of polar-orbiting sensors (e.g., Advanced Very High Resolution Radiometer and Moderate Resolution Imaging Spectroradiometer). In this paper, we discuss the development of a split window LST algorithm for the ABI sensor. First, we simulated ABI sensor data using the MODTRAN radiative transfer model and NOAA88 atmospheric profiles. To model land conditions, we developed emissivity data for 78 virtual surface types using the surface emissivity library from Snyder *et al.* Using the simulation results, we performed regression analyses with the candidate LST algorithms. Algorithm coefficients were stratified for dry and moist atmospheres as well as for daytime and nighttime conditions. We estimated the accuracy and sensitivity of each algorithm for different sun-view geometries, emissivity errors, and atmospheric assessments. Finally, we evaluated the most promising algorithm using real data from the GOES-8 Imager and SURFace RADiation Network. The results indicate that the optimized LST algorithm meets the required accuracy (2.3 K) of the GOES-R mission.**

***Index Terms*—Advanced Baseline Imager (ABI), Geostationary Operational Environmental Satellite (GOES), land surface temperature (LST), split window (SW).**

Manuscript received February 15, 2008; revised May 20, 2008 and September 4, 2008. First published December 9, 2008; current version published February 19, 2009.

Y. Yu is with the National Environmental Satellite, Data, and Information Service Center for Satellite Applications and Research, National Oceanic and Atmospheric Administration, Camp Springs, MD 20746 USA (e-mail: Yunyue.Yu@noaa.gov).

D. Tarpley is with Short & Associates, Camp Springs, MD 20746 USA (e-mail: Dan.Tarpley@noaa.gov).

J. L. Privette is with the National Environmental Satellite, Data, and Information Service National Climatic Data Center, National Oceanic and Atmospheric Administration, Asheville, NC 28801 USA (e-mail: jeff.privette@noaa.gov).

M. D. Goldberg is with the National Environmental Satellite, Data and Information Service Center for Satellite Applications and Research, National Oceanic and Atmospheric Administration, Camp Springs, MD 20746 USA (e-mail: Mitch.Goldberg@noaa.gov).

M. K. Rama Varma Raja and H. Xu are with I. M. Systems Group, Inc., Camp Springs, MD 20746 USA (e-mail: Rama.Mundakkara@noaa.gov; Hui.Xu@noaa.gov).

K. Y. Vinnikov is with the Department of Atmospheric and Oceanic Science, University of Maryland, College Park, MD 20742 USA (e-mail: kostya@atmos.umd.edu).

Digital Object Identifier 10.1109/TGRS.2008.2006180

I. Introduction

LAND SURFACE temperature (LST), as a key indicator of the Earth's surface energy budget, is widely required in applications of hydrology, meteorology, and climatology [1], [2]. Satellite LSTs have been routinely produced from imagery data of geostationary and polar-orbiting satellites. By 2010, more than 30 years of global satellite LST data will be available, which will provide a rich archive with which climate data records can be developed and analyzed for climate change signals.

The National Oceanic and Atmospheric Administration (NOAA) has operated the Geostationary Operational Environmental Satellite (GOES) program for more than 30 years. From the earliest days of the program, GOES imagery data were used for a variety of tasks, such as tracking hurricanes and volcano ash as well as deriving cloud drift winds and their temperatures [3], [4]. Starting with the GOES-8 satellite, launched in April 1994, many investigators have studied operational LST algorithms for use with the Imagers [5]–[8]. Although the spatial resolution (up to 4 km) of the current Imager is significantly lower than that of polar-orbiting satellite sensors (e.g., 1.1 km for Advanced Very High Resolution Radiometer (AVHRR) and 1 km for Moderate Resolution Imaging Spectroradiometer (MODIS) of the Earth Observing System), the GOES Imagers provide hourly measurements over the hemisphere which is a unique data source for studies of the Earth's diurnal variability.

NOAA is developing a new generation of GOES satellites, the GOES-R series, which will provide timely and accurate Earth surface measurements through an Advanced Baseline Imager (ABI) [9]. Compared to the current GOES Imager, the ABI's performance will be more like that of polar-orbiting satellite sensors, such as AVHRR, in terms of spatial resolution (up to 2 km) and noise equivalent temperature (0.1 K in thermal infrared channels). The ABI's data refresh rate will be 5 min, which is a significant improvement over the 15 min of the GOES Imager.

The ABI sensor will have 16 channels over the visible and infrared wavelengths. Channels 14 and 15, centered at the wavelengths 11.2 and 12.3 μm, respectively, are most applicable for land and sea surface temperature (SST) retrieval. These bands are in the thermal infrared spectral range that features high surface emission and atmospheric transparency [10]. As noted in [11] and [12], the radiation signal difference between the two channels provides a very good atmospheric correction, a feature exploited by the split window (SW) class of LST algorithms.

TABLE I

CANDIDATE SW LST ALGORITHMS AS USED IN THIS STUDY. EACH CANDIDATE ALGORITHM CONSISTS OF TWO PARTS: 1) THE BASE SW ALGORITHM AND 2) THE ADDED PATH LENGTH CORRECTION (THE LAST TERM IN EACH ALGORITHM). THE BASE ALGORITHMS ARE ADAPTED FROM THE PUBLICATIONS LISTED UNDER "REFERENCE FOR BASE ALGORITHM," WHILE THE PATH LENGTH TERM WAS ADDED IN THE PRESENT STUDY TO PROVIDE IMPROVED ANGULARLY VARYING ATMOSPHERIC CORRECTION

No	Candidate Algorithm#	Reference for Base Algorithm Adaptation
1	$T_s = C + (A_1 + A_2 \frac{1-\varepsilon}{\varepsilon} + A_3 \frac{\Delta\varepsilon}{\varepsilon^2})(T_{11} + T_{12}) + (A_4 + A_5 \frac{1-\varepsilon}{\varepsilon} + A_6 \frac{\Delta\varepsilon}{\varepsilon^2})(T_{11} - T_{12}) + D(T_{11} - T_{12})(\sec\theta - 1)$	Wan & Dozier [19]; Becker & Li [20]
2	$T_s = C + A_1 \frac{T_{11}}{\varepsilon} + A_2 \frac{T_{12}}{\varepsilon} + A_3 \frac{1-\varepsilon}{\varepsilon} + D(T_{11} - T_{12})(\sec\theta - 1)$	Prata & Platt [21]; modified by Caselles *et al.* [22]
3	$T_s = C + A_1 T_{11} + A_2(T_{11} - T_{12}) + A_3(1 - \varepsilon_{11}) + A_4 \Delta\varepsilon + D(T_{11} - T_{12})(\sec\theta - 1)$	Ulivieri *et al.* [27]
4	$T_s = C + A_1 T_{11} + A_2(T_{11} - T_{12}) + A_3 \frac{1-\varepsilon}{\varepsilon} + A_4 \frac{\Delta\varepsilon}{\varepsilon^2} + D(T_{11} - T_{12})(\sec\theta - 1)$	Vidal [23]
5	$T_s = C + A_1 T_{11} + A_2(T_{11} - T_{12}) + A_3(T_{11} - T_{12})\varepsilon_{11} + A_4 T_{12} \Delta\varepsilon + D(T_{11} - T_{12})(\sec\theta - 1)$	Price [24].
6	$T_s = C + A_1 T_{11} + A_2(T_{11} - T_{12}) + A_3 \varepsilon + D(T_{11} - T_{12})(\sec\theta - 1)$	Uliveri & Cannizzaro [25]
7	$T_s = C + A_1 T_{11} + A_2(T_{11} - T_{12}) + A_3 \varepsilon + A_4 \frac{\Delta\varepsilon}{\varepsilon} + D(T_{11} - T_{12})(\sec\theta - 1)$	Sobrino *et al.* [26]
8	$T_s = C + A_1 T_{11} + A_2(T_{11} - T_{12}) + A_3(1 - \varepsilon) + A_4 \Delta\varepsilon + D(T_{11} - T_{12})(\sec\theta - 1)$	Ulivieri *et al.* [27]
9	$T_s = C + A_1 T_{11} + A_2(T_{11} - T_{12}) + A_3(T_{11} - T_{12})(T_{11} - T_{12}) + A_4(1 - \varepsilon_{11}) + A_5 \Delta\varepsilon + D(T_{11} - T_{12})(\sec\theta - 1)$	Coll *et al.* [28]

#Note:
1) T_{11} and T_{12} represent the top-of-atmosphere brightness temperatures of ABI channels 14 and 15, respectively;
2) $\varepsilon=(\varepsilon_{11}+\varepsilon_{12})/2$ and $\Delta\varepsilon=(\varepsilon_{11}-\varepsilon_{12})$, where ε_{11} and ε_{12} are the spectral emissivity values of the land surface at ABI channels 14 and 15, respectively;
3) θ is the satellite view zenith angle.

In this study, we attempted to determine an optimal LST algorithm for the ABI sensor. Specifically, we sought to identify an SW LST algorithm that is not just suitable for the GOES-R program but to serve the long term data record needs for climate change study [13]. That said, the developed algorithm should be applicable to the polar-orbiting satellite sensor, and the GOES-R LSTs should be consistent with the LSTs produced from the polar-orbiting satellite data [14].

The outline of this paper is as follows. In Section II, we describe the SW LST algorithms evaluated in this study. In Section III, we test and analyze the algorithms using MODTRAN radiative transfer simulation model and evaluate a selected algorithm using GOES-8 Imager data and ground measurements. The results of the simulation test and analyses, and the corresponding satellite and ground data comparisons, are presented in Section IV. The discussion of issues and considerations are given in Section V. Finally, we present concluding remarks in Section VI.

II. CANDIDATE ALGORITHMS

Satellite LST retrievals are usually performed in thermal infrared bands where the surface emission reaches its maximum; yet, atmospheric absorption is small. Although several other methods have been published (e.g., [15] and [16]), the SW method is most frequently used. McMillin [17] found that the atmospheric absorption in thermal wavebands could be corrected using the signal difference between two adjacent channels. This "SW" technique has been successfully applied for SST for more than 20 years. Its use for land has lagged that for oceans given the additional challenges in characterizing land surface emissivity. Nevertheless, the SW technique is a good choice for GOES-R since it is simple and robust for operational use yet is sufficiently accurate to meet mission requirements [18].

We considered nine SW LST algorithms from the literature [14], [19]–[28] and adapted these (Table I) to be candidate algorithms for the ABI. Each algorithm consists of a "base" SW algorithm plus a path length correction. The base algorithms represent those adapted from the literature. We added a path length correction, which is the last term in each algorithm, for additional atmospheric correction [12], [29]. Geometric analysis shows that the atmospheric path length at 60° of the satellite zenith angle is about two times larger than at the nadir. Yu *et al.* [14] showed that, if an algorithm's coefficients are determined for typical column water vapor amounts, algorithm accuracy can degrade significantly at large view angles unless a corrective term is applied. Therefore, we used the term $(T_{11} - T_{12})(\sec\theta - 1)$ for path length correction. A detailed description of this term is in [14].

Note that, within the GOES-R program, potential LST retrieval approaches must use emissivity data determined *a priori*

[18]. Some SW LST algorithms (e.g., those of [5], [6], and [21]) use such emissivity information indirectly through the use of different coefficient sets determined for different land surface types. However, such approaches cannot readily address within-class variability which can be as great as or greater than between-class variability. Therefore, we chose to consider only emissivity explicit algorithms (i.e., those with spectral emissivity specified as an independent variable) since these allow the easy incorporation of updated emissivity (or land cover) maps [e.g., annual maps from the Earth Observing System/MODIS or the planned updates from National Polar-orbiting Operational Environmental Satellite System/Visible/Infrared Imager Radiometer Suite (VIIRS)]. These also permit emissivity maps that address within-class variability [30] and could potentially use emissivity databases that include directional variability [31] should they become available in the GOES-R era.

III. Algorithm Selection

To select a suitable algorithm for the GOES-R ABI, we analyzed the accuracy and sensitivity of the aforementioned SW algorithms using a comprehensive simulation data set. The accuracy of the best performing algorithm was further studied using ground LST data from the SURFace RADiation (SURFRAD) network data and corresponding GOES-8 satellite data. We discuss these two analysis approaches in the following sequence.

A. Simulation Model and Processes

The MODTRAN atmospheric radiative transfer model [32] has been widely used in satellite remote sensing studies. MODTRAN is a moderate spectral resolution model up to cm^{-1} in frequency. We used MODTRAN version 4, reversion 2, released in 2000.

We varied MODTRAN's model atmosphere using 126 atmospheric temperature/water vapor profiles: 60 for daytime and 66 for nighttime. The profiles were determined from cloud-free radiosonde data available from the Cross-track InfraRed Sounder F98-Weather Products Test Bed Data Package (NOAA88, Rev. 1.0). The profiles represented a variety of atmospheric conditions, spanning a column water vapor range from 0.2 to 7.5 g/cm^2 and a surface air temperature range from 240 K to 306 K. The profiles are fairly evenly distributed over their ranges as shown in Fig. 1. The profiles spanned a latitude range from 60° south to 70° north.

To simulate a wide range of environmental conditions using a limited profile set, we followed Yu *et al.* [31] and varied the prescribed LST for each profile in a range as $T_{\mathrm{air}} - 15 <$ LST $< T_{\mathrm{air}} + 15$ K, where T_{air} is the surface air temperature of the profile, with a 1-K increment. The ±15-K difference range includes most, but not all (e.g., some semiarid environments in some situations), conditions in nature. For each prescribed LST, we iterated the prescribed sensor view zenith angle from 0° to 70°.

To address natural land variability, we generated top-of-atmosphere radiances for 78 land cover cases as represented by different spectral emissivity pairs (i.e., sets of 11.2- and 12.3-μm emissivity values). We determined the pairs using the emissivity classification data of Snyder *et al.* [33]. Of those,

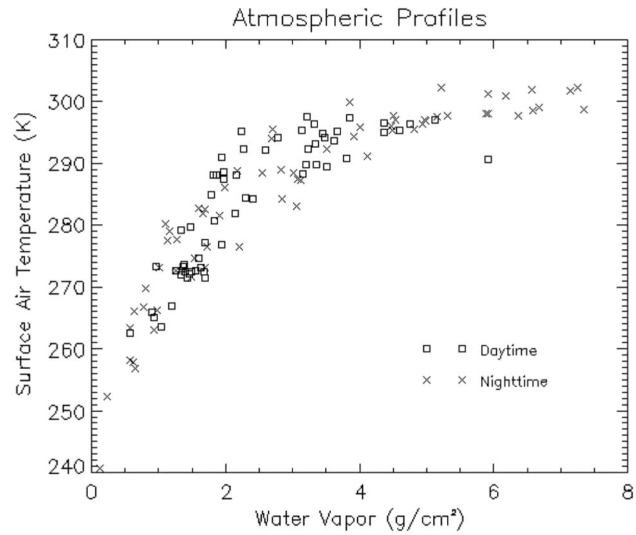

Fig. 1. Water vapor and surface air temperature distribution of the 126 atmospheric profiles used in the simulation analyses.

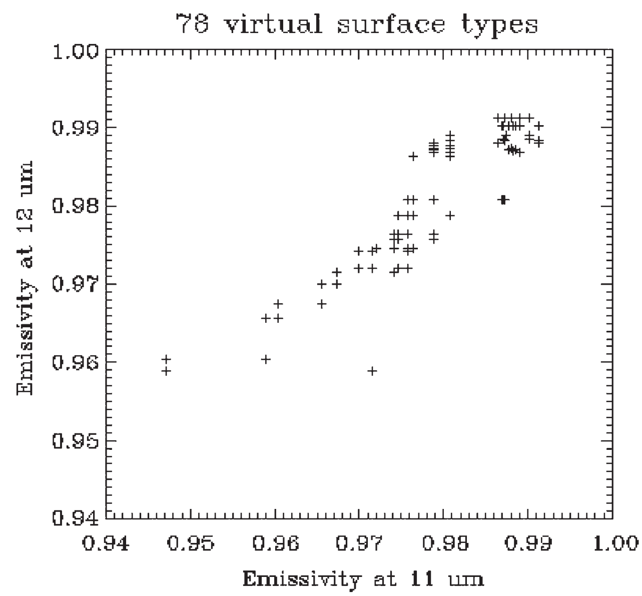

Fig. 2. Distribution of emissivity values at the ∼11- and ∼12-μm spectral channels. A total of 78 emissivity pairs were used in the simulation and regression analyses.

14 represent the means of Snyder's 14 surface classes, and 12 are those values combined with the estimated uncertainties (duplicates were eliminated). To specify additional cases, we recombined the 11- and 12-μm emissivity values and constructed an additional 52 "virtual surface types." Each virtual surface type was carefully assessed manually against the variability in Snyder's original samples to ensure that the virtual types were realistic and yet had adequate variation. Fig. 2 shows the emissivity distribution of the 78 virtual surface types. Following most prior studies in the literature, we assumed angularly isotropic emissivity. This stems from the relative lack of information on emissivity directionality and, likely, does not impact the results of the present study.

Upon simulating the top-of-atmosphere radiances, we determined the mean channel radiance by integrating over the sensor spectral response function (SRF). The channel radiances were converted into corresponding brightness temperatures using the Planck function. Because ABI is still in development, measured SRFs are not currently available. Instead, the GOES-R Algorithm Working Group (AWG) has recommended a "Gaussian Boxcar Hybrid" function as SRFs of the ABI for corresponding algorithm development uses. We expect that using modeled, rather than measured, SRFs will not significantly affect our results since Yu *et al.* [14] demonstrated that the SW LST algorithms are not very sensitive to SRF variations in the thermal infrared channels.

After running the MODTRAN simulations with iterations of atmospheric profiles, surface temperatures, and view zenith angles, we obtained 9840 daytime data pairs (where a "pair" represents the prescribed LST and the associated modeled brightness temperatures in ABI channels 14 and 15) and 10 660 nighttime data pairs for each emissivity value.

B. Regression Analyses

Because water vapor is the most significant atmospheric absorber in the thermal bands, we stratified the simulation data according to the water vapor content: 1) "dry" atmosphere, where the total column water vapor is less than 2.0 g/cm^2, and 2) "moist" atmosphere, where the water vapor content is larger than 2.0 g/cm^2. Similar data stratification was used in the official MODIS LST algorithm [19]. The stratification acknowledges the capacity of warm atmospheres to hold more water vapor, as shown in Fig. 1, and the degradation of LST algorithm performance with increasing water vapor.

Due to significant differences in the discontinuity between LST and air temperature, during daytime and nighttime, many LST retrieval algorithms (or accompanying coefficient sets) were specified uniquely for daytime or nighttime use. We also performed regressions separately for the daytime and nighttime data sets. In addition, to better simulate real satellite data, we added Gaussian-distributed random noise to both the simulated brightness temperatures and surface emissivity values. The standard deviations (STDs) of the sensor noise equivalent delta temperature (NEDT) and the surface emissivity noise are 0.1 K and 0.005 (unitless), respectively. The NEDT value is the design requirement for ABI in channels 14 and 15; the emissivity noise STD is 2.5 times the digitization error of the MODIS emissivity product, which will be a resource in the ABI LST derivation.

Before conducting regression analysis with the simulated data and candidate algorithms, we also considered the natural Gaussian-like distribution of land surface and surface air temperatures as noted by Justin *et al.* (NGST technical report, personal communication, 2006). That report used National Centers for Environmental Prediction and European Center for Medium-range Weather Forecasts data sets for VIIRS LST algorithm analysis. We therefore applied a Gaussian function to filter the simulation data before running the algorithm regression process. Fig. 3 shows the filtering results for the daytime data set. A similar process was applied on the nighttime data set.

C. Sensitivity Analyses

Two important error sources in LST retrieval are the surface emissivity uncertainty and the atmospheric water vapor absorption. We therefore analyzed the sensitivities of the candidate LST algorithms (Table I) to those two factors.

1) Emissivity Uncertainty: Analytically, the maximum LST uncertainty δT_s due to the emissivity uncertainty can be described as

$$\delta T_s = \sqrt{\delta T_1^2 + \delta T_2^2} \tag{1}$$

where δT_1 and δT_2 represent the 11- and 12-μm band uncertainties resulting from the uncertainties of the mean emissivity (ε) and emissivity difference ($\Delta\varepsilon$), respectively. Using algorithm 7 (Table I) as an example, these two components are

$$\delta T_1 = \left(A_3 - \frac{A_4}{\varepsilon^2}\right)\delta\varepsilon \qquad \delta T_2 = \frac{A_4}{\varepsilon}\delta(\Delta\varepsilon). \tag{2}$$

Therefore, the maximum LST uncertainty for algorithm 7 is

$$\delta T_s = \sqrt{\left(\left(A_3 - \frac{A_4}{\varepsilon^2}\right)\delta\varepsilon\right)^2 + \left(\frac{A_4}{\varepsilon}\delta(\Delta\varepsilon)\right)^2}. \tag{3}$$

Considering that $\varepsilon = (\varepsilon_{11} + \varepsilon_{12})/2$ and $\Delta\varepsilon = (\varepsilon_{11} - \varepsilon_{12})$ and assuming that the emissivity uncertainties in each band are the same, i.e., $\delta\varepsilon = \delta\varepsilon_{11} = \delta\varepsilon_{12}$, the maximum uncertainty of the emissivity difference is $\delta(\Delta\varepsilon) = |\delta\varepsilon_{11}| + |\delta\varepsilon_{12}| = 2\delta\varepsilon$. Thus, the LST uncertainty δT_s due to the emissivity uncertainty can be calculated using the equation previously shown.

2) Water Vapor Uncertainty: Stratifying our regressions by water vapor regime, we assume that water vapor content can be well estimated *a priori*. In practice, water vapor information is usually available from satellite soundings, ground radiosondes, and/or operational numerical weather prediction model forecasts. Nevertheless, two errors may occur. First, the water vapor value may be mismeasured due to a variety of error sources. Second, due to spatial resolution differences between the ABI and water vapor data, both dry and moist atmospheric conditions may occur within the unit spatial area over which the water vapor was estimated (which may contain from several to more than ten GOES-R pixels). Therefore, the coefficient set of the LST algorithm for dry atmospheres may be incorrectly applied in a moist atmospheric condition and vice versa. To test the sensitivity of the algorithms to this error, we applied the algorithm coefficient sets derived for moist atmospheres to dry atmospheric conditions and vice versa.

In addition, the GOES-R sensor view geometry may have significant impact on the variation of atmospheric absorption due to the radiative transfer path length increase from nadir to the edge of the scan. Considering that the altitude of GOES-R satellite is about 36 000 km and the Earth radius is about 6700 km, the relationship between the satellite zenith angle (θ) and the satellite viewing angle (θ_v) is [6]

$$\begin{aligned}\sin\theta &= \frac{\text{Satellite Altitude} + \text{Earth Radius}}{\text{Earth Radius}}\sin\theta_v \\ &\approx 6.37\sin\theta_v.\end{aligned} \tag{4}$$

Therefore, the maximum satellite viewing angle (about 8.7°) corresponds to 74.48° of view zenith angle. Such a large view zenith angle may have great impact on LST retrieval since, for instance, when the zenith angle is increased from 0° to 60°,

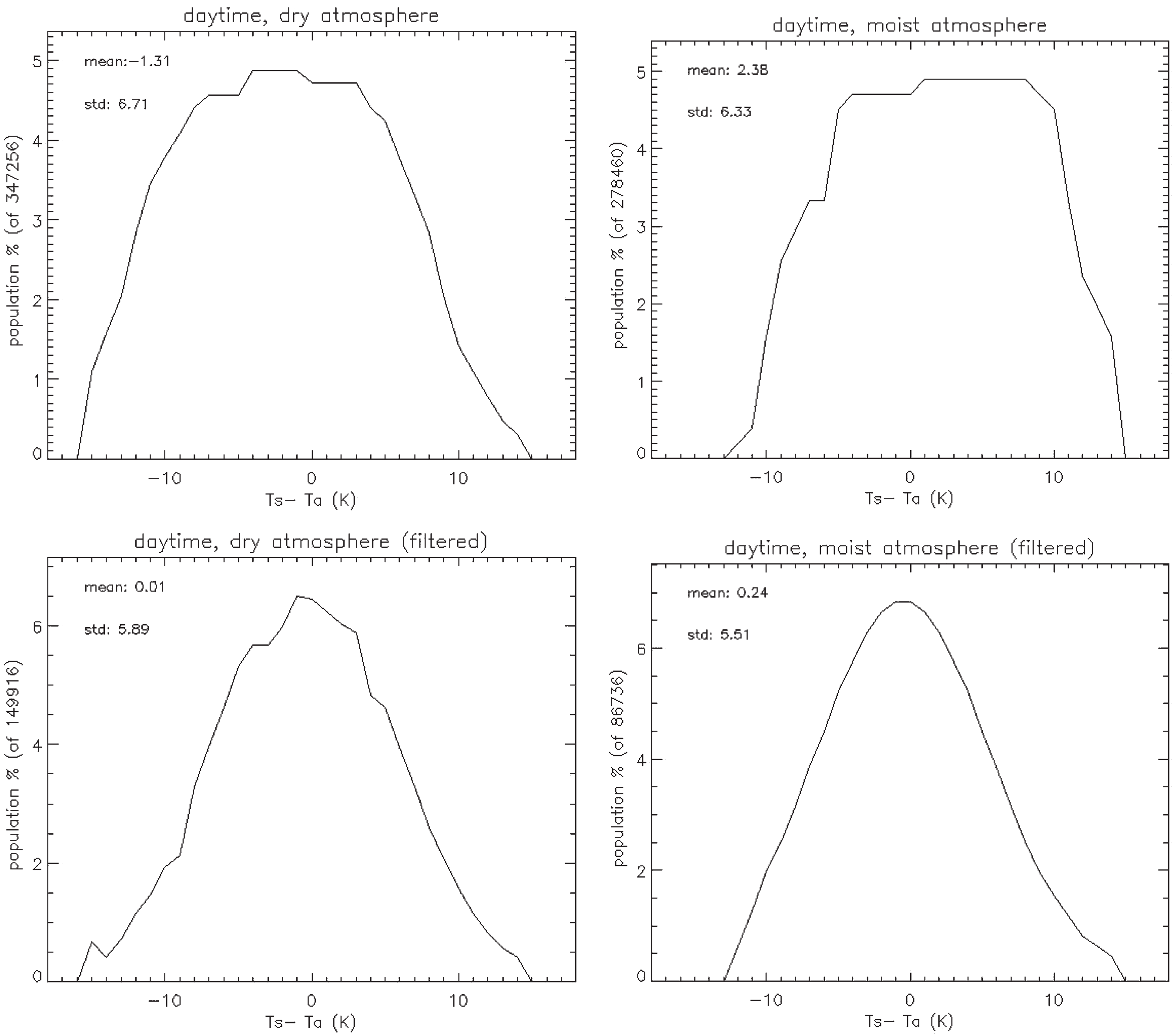

Fig. 3. Daytime simulation data distribution in terms of the land surface and surface air temperature differences (Ts - Ta). (Upper panels) The original simulation data are pretty much evenly distributed in a range of the temperature differences. The filtered data for both the (left) dry and (right) moist atmospheres are shown in the bottom panels.

the atmospheric path length is doubled. We therefore assessed candidate algorithm sensitivity to the varying zenith angles using the simulation data sets.

D. Ground Evaluation

To evaluate the best performing GOES-R LST algorithm, we collected ground LST data estimated from SURFRAD stations and the corresponding GOES-8 Imager data. The GOES-8 Imager provides an excellent proxy for GOES-R ABI since it has similar channels at 11- and 12-μm wavelengths.

The SURFRAD network has been operational in the United States since 1995. It provides high quality *in situ* measurements of upwelling and downwelling radiation, along with other meteorological parameters. A detailed description of the SURFRAD network and associated instrumentation can be found in [34] and [35]. We used one year (2001) of SURFRAD data over six sites as described in Table II. Surface-type information for the sites, which were used to estimate the surface emissivity, was obtained from the University of Maryland (UMD) land classification data set [36].

TABLE II
LOCATION AND SURFACE TYPES OF THE SIX SURFRAD SITES

Site No.	Site Location	LAT, LONG	Surface Type#
1	Pennsylvania State University, PA	40.72N, -77.93W	Mixed Forest
2	Bondeville, IL	40.05N, -88.37W	Crop Land
3	Goodwin Creeks, MS	34.25N, -89.87W	Evergreen Needle Leaf Forest
4	Fort Peck, MT	48.31N, -105.10W	Grass Land
5	Boulder, CO	40.13N, -105. 24W	Crop Land
6	Desert Rock, NV	36.63N, -116.02 W	Open Shrub Land

#: UMD land surface type.

The SURFRAD ground LST values were calculated from upwelling and downwelling radiation measurements obtained by a precise infrared radiometer (PIR), in a spectral range from 3 to 50 μm. The SURFRAD PIR is calibrated annually using a laboratory blackbody such that its measurement estimates the total energy emitted from a blackbody rather than the instrument limited spectrum [34], [35]. The surface radiant exitance Φ_e can be estimated using

$$\Phi_e = \Phi_u - (1 - \varepsilon)\Phi_d \tag{5}$$

where Φ_u and Φ_d are the upwelling and downwelling fluxes, respectively, and ε is the broadband surface emissivity [36], [37]. The surface temperature T_s can be derived using Stefan–Boltzmann equation

$$\Phi_e = \varepsilon\sigma T_s^4 \tag{6}$$

where σ is the Stefan–Boltzmann constant which has a value of $5.67051 \times 10^{-8}\ \mathrm{W} \cdot \mathrm{m}^{-2} \cdot \mathrm{K}^{-4}$.

The emissivity in (6) was estimated by mapping the UMD surface-type classification to the land surface emissivity classification of Snyder *et al.* The mapping method is described in [31]. Note that the mapped emissivities are spectral emissivity values at around 11 and 12 μm (the SW channels). We assumed that the mean broadband emissivity of the channel emissivities is applicable to (6); discussion of such assumption and possible error may be found in [37].

The SURFRAD measurements are effectively point measurements, as we did not attempt to mathematically scale their value to areas commensurate with GOES-8 imagery pixels. This disparity can lead to both systematic and nonsystematic differences between GOES-8 and SURFRAD values for the same time. This problem is reduced for homogeneous areas; however, we did not quantitatively assess the homogeneity of these sites for this study.

The GOES-8 Imager data was provided by the GOES-R AWG proxy data team. It is 4 km in spatial resolution and 1 h in temporal resolution. In this study, we selected the Imager pixels that were spatially nearest to the SURFRAD locations. In the time domain, we used only the SURFRAD values that were closest to the GOES-8 measurements. The maximum temporal difference between the SURFRAD and the satellite measurements was less than 2 min since the SURFRAD daily files provide measurements every 3 min.

An accurate cloud filter for the Imager data is critical to reliable results. To minimize cloudy data, we performed a manual cloud filtering procedure instead of using automated cloud filtering algorithms. The approach included the manual assessment of the following quantities:

1) channel 1 reflectance normalized by the cosine of solar zenith angle;
2) channel 4 brightness temperature;
3) daily time series of solar irradiance measured at the SURFRAD site;
4) daily time series of downwelling sky irradiance measured at the SURFRAD site;
5) STD of 3 by 3 pixel channel 4 brightness temperatures;
6) difference between SURFRAD LST and the match-up GOES-8 pixel channel 4 brightness temperature;
7) channel 4 and 5 brightness temperature difference of the match-up pixel;
8) channel 4 and 2 brightness temperature difference of the match-up pixel.

TABLE III
MATCH-UP DATA NUMBERS OF SURFRAD SITES

Month	Site 1		Site 2		Site 3		Site 4		Site 5		Site 6	
	Day	Night	Day	Night	Day	Night	Day	Night	Day	Night	Day	Night
1	16	33	46	69	76	154	57	124	84	157	113	245
2	17	45	9	28	36	86	78	139	35	95	96	135
3	0	0	33	92	70	94	77	125	23	58	145	141
4	66	84	28	42	63	89	25	64	44	67	112	74
5	40	69	21	31	107	134	90	64	51	43	158	190
6	26	39	37	54	37	83	27	32	49	64	235	189
7	1	8	34	56	31	48	14	22	48	34	250	226
8	16	33	35	69	12	47	106	106	39	64	188	195
9	46	83	70	110	84	102	69	76	97	123	226	257
10	56	77	66	101	156	213	39	67	28	75	96	152
11	59	118	84	148	47	112	32	94	110	176	85	147
12	25	54	35	99	61	148	38	133	73	124	58	72

First, the images of channel 1 reflectance (center wavelength: 0.635 μm) and channel 4 brightness temperature (center wavelength: 10.694 μm) were checked to determine if there was any sign of clouds in the SURFRAD station pixel and its surrounding area (about 0.5° by 0.5°). In general, most clouds cause enhanced reflectance and lower brightness temperatures (except the low-level warm clouds) relative to the surface. Snow conditions can be identified from image sequences, since snow pixels generally tend to be static from one hour to the next hour while clouds move.

Second, in general, if the channel 4 brightness temperature is too low (less than 250 K), then most likely, the pixel is under cloud influences. For a pixel to be considered "clear," the absolute difference of the channel 4 brightness temperature and the SURFRAD LST should be, in general, less than 10 K. For most clear skies, the STD of the nearby 3 by 3 pixel array must be less than 1.5 K, although it maybe slightly higher (e.g., 1.75 K) for sites like Boulder. In addition, the absolute brightness temperature difference between channels 4 and 5 (center wavelength: 11.965 μm) and channels 4 and 2 (center wavelength: 3.9 μm) should be, in general, less than 1.5 K, for identifying the pixel as cloud free.

Apart from the satellite data, the SURFRAD ground measurements were also used in the cloud filtering. For most cloud-free (or cloudy) conditions, during daytime, the solar irradiance temporal profile is a smoothly (or highly irregular) varying curve, except when thin clouds occur which have very little effect on the variation of solar irradiance. In most of these exceptional circumstances, the sky downwelling irradiance profile shows enhancements which enable the detection of clouds.

We determined cloud conditions using all of the filters aforementioned, although it was very time consuming. Note that, during nighttime, only the infrared channels of the satellite data and the downwelling sky irradiance of the SURFRAD data were used for the cloud filtering. Table III indicates the number of match-up data pairs (with both SURFRAD and GOES measurements) for each site in each month of the year 2001. Except in March and July at site 1 (Pennsylvania State University in State College, PA), each site/month/diurnal phase combination is well represented (at least nine observations, typically many more).

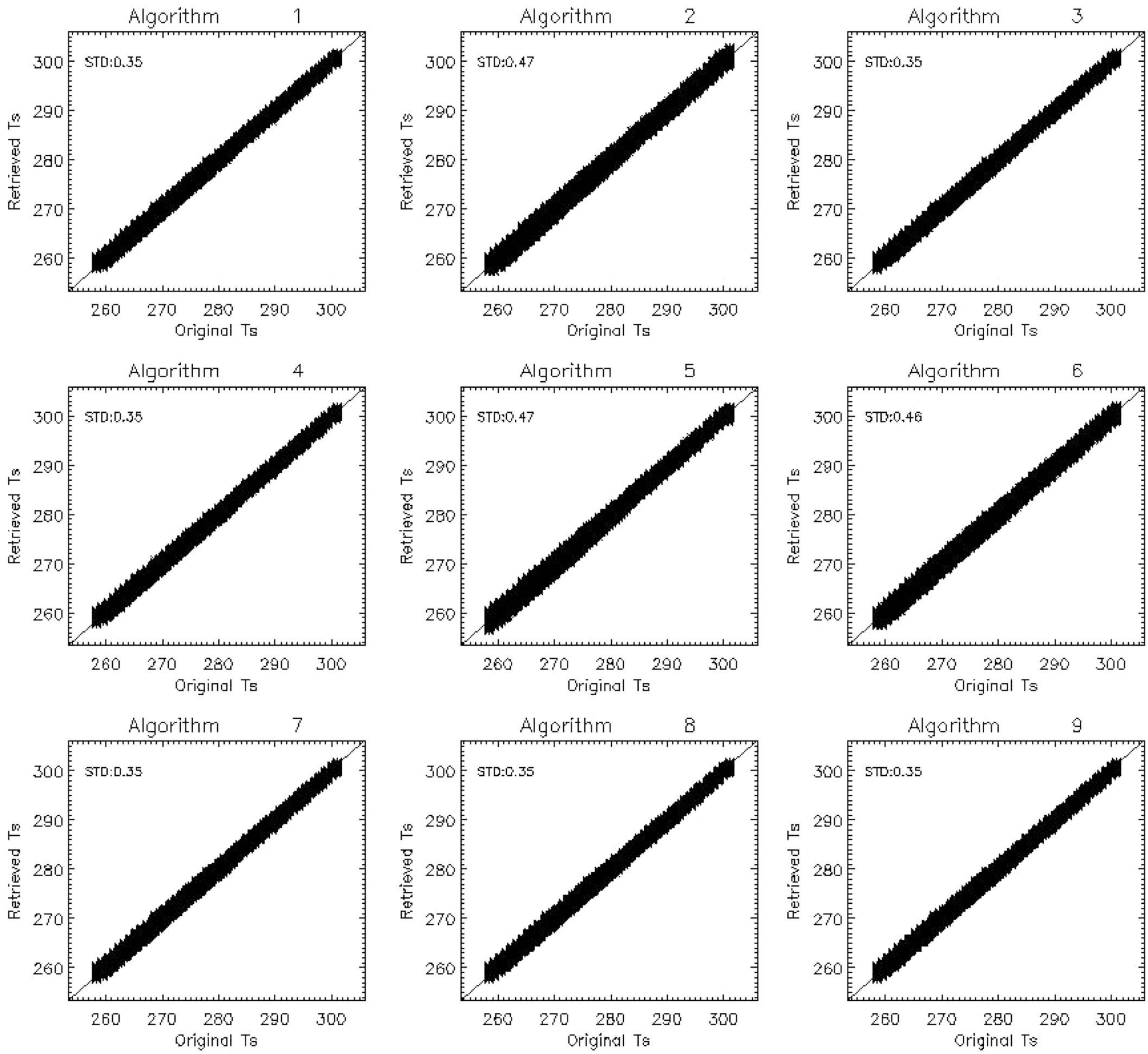

Fig. 4. Scatter gram plots of the regression results for the dry atmosphere (daytime). STD errors of the regression are given in each plot.

Finally, to estimate LST from the GOES Imager data, we used the LST algorithm which performed best in the MODTRAN simulation analyses described previously. As before, we used algorithm coefficients determined through regression with the MODTRAN simulation data set and the GOES-8 Imager SRFs.

IV. Results

For determining the most suitable ABI LST algorithm, we compared the performance of the algorithms listed in Table I for dry and moist atmospheric conditions as well as for daytime and nighttime scenarios. The performance is assessed by considering the algorithm accuracy and sensitivity. The SURFRAD evaluation for the best performing algorithm was used to determine of the algorithm would meet GOES-R requirements.

TABLE IV
STD Errors (Kelvins) of the Regression Analysis

No	Daytime		Nighttime	
	Dry	Moist	Dry	Moist
1	0.35	0.70	0.32	0.92
2	0.47	0.75	0.47	0.96
3	0.35	0.70	0.33	0.92
4	0.35	0.70	0.32	0.92
5	0.47	0.72	0.47	0.94
6	0.46	0.75	0.45	0.95
7	0.35	0.70	0.33	0.92
8	0.35	0.70	0.33	0.92
9	0.35	0.65	0.31	0.89

A. Algorithm Accuracy

For each of the nine algorithms, we calculated the bias and STD of the regressions. Fig. 4 shows the scatter plots of the

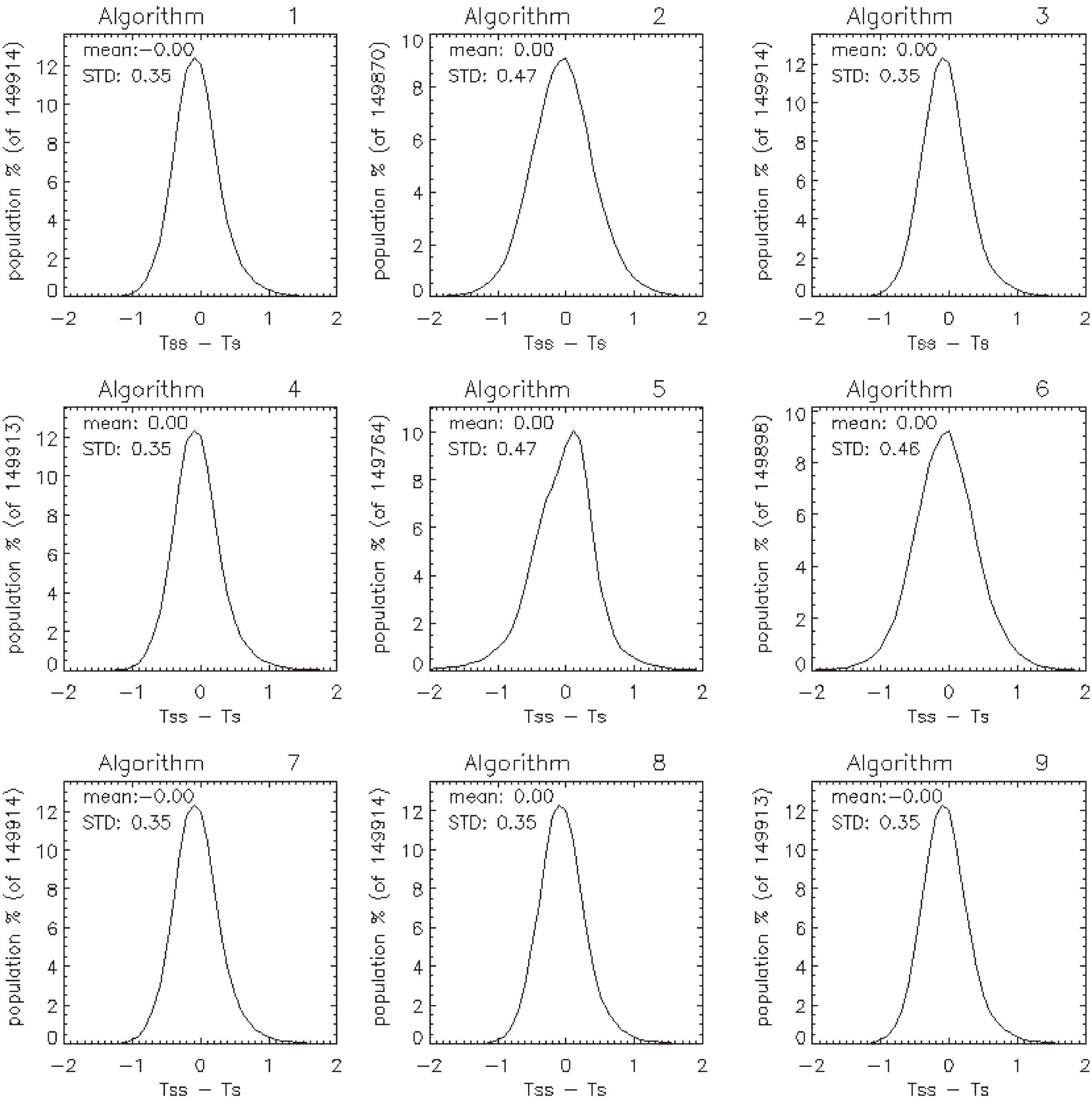

Fig. 5. Histogram plots of the regression results for the dry atmosphere (daytime). Tss is the retrieved LST, and Ts is the true LST. STD of the difference and mean difference of the regression are given in each plot.

regression results for the daytime dry atmosphere cases. It indicates that all algorithms perform well for an LST range from about 255 K to 305 K. The STD of the differences between the prescribed LSTs and the retrieved LSTs ranged from 0.35 K (algorithms 1, 3, 4, 7, 8, and 9) to 0.47 K (algorithms 2 and 5). Similar accuracy is observed for the moist atmosphere cases, where the STD ranged from 0.65 K (algorithm 9) to 0.75 K (algorithms 2 and 6). For the nighttime cases, similar regression accuracies are observed. STDs of the algorithms under different atmospheric conditions are listed in Table IV.

To have a closer look at error distributions, we produced histogram plots of the regression fits. Fig. 5 shows an example for the daytime dry atmosphere cases. All the histogram plots reveal that there is no significant bias in any of the algorithms, and the error distributions are fairly symmetric (Gaussian-distribution-like) around zero. That means all algorithms performed well, and the retrieval noise level (less than 1.0 K) is smaller than the GOES-R mission requirements document (MRD) requirement. Note that, since the regression bias is zero for all the algorithms, the STD equals the accuracy of the regression statistics. We therefore used the STD as the accuracy metric in the simulation analyses.

Compared to the daytime algorithm performance, the STD of the nighttime for the moist atmosphere cases is

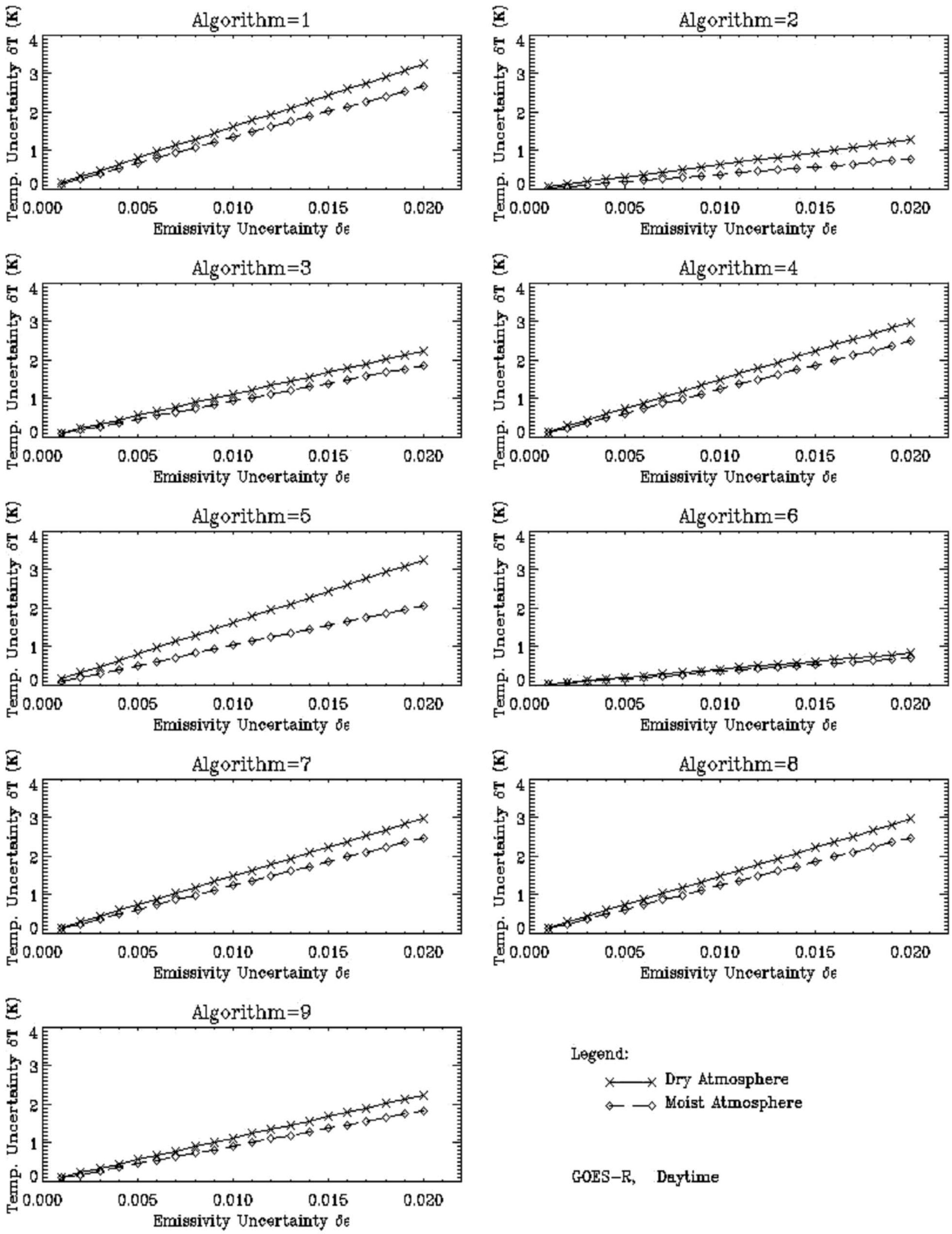

Fig. 6. Uncertainty of the retrieved LSTs along with the surface emissivity uncertainty. Daytime algorithms. In the plots, it is assumed that the mean emissivity $\varepsilon = 0.97$, the emissivity difference $\Delta\varepsilon = 0.005$, and the surface temperature is at about 298 K.

slightly worse for each algorithm. This is because the nighttime atmospheric profiles used in the simulation process are moister than the daytime atmospheric profiles, as shown in Fig. 1. For the dry atmosphere cases, the regression STD of each algorithm is fairly similar between the daytime and nighttime.

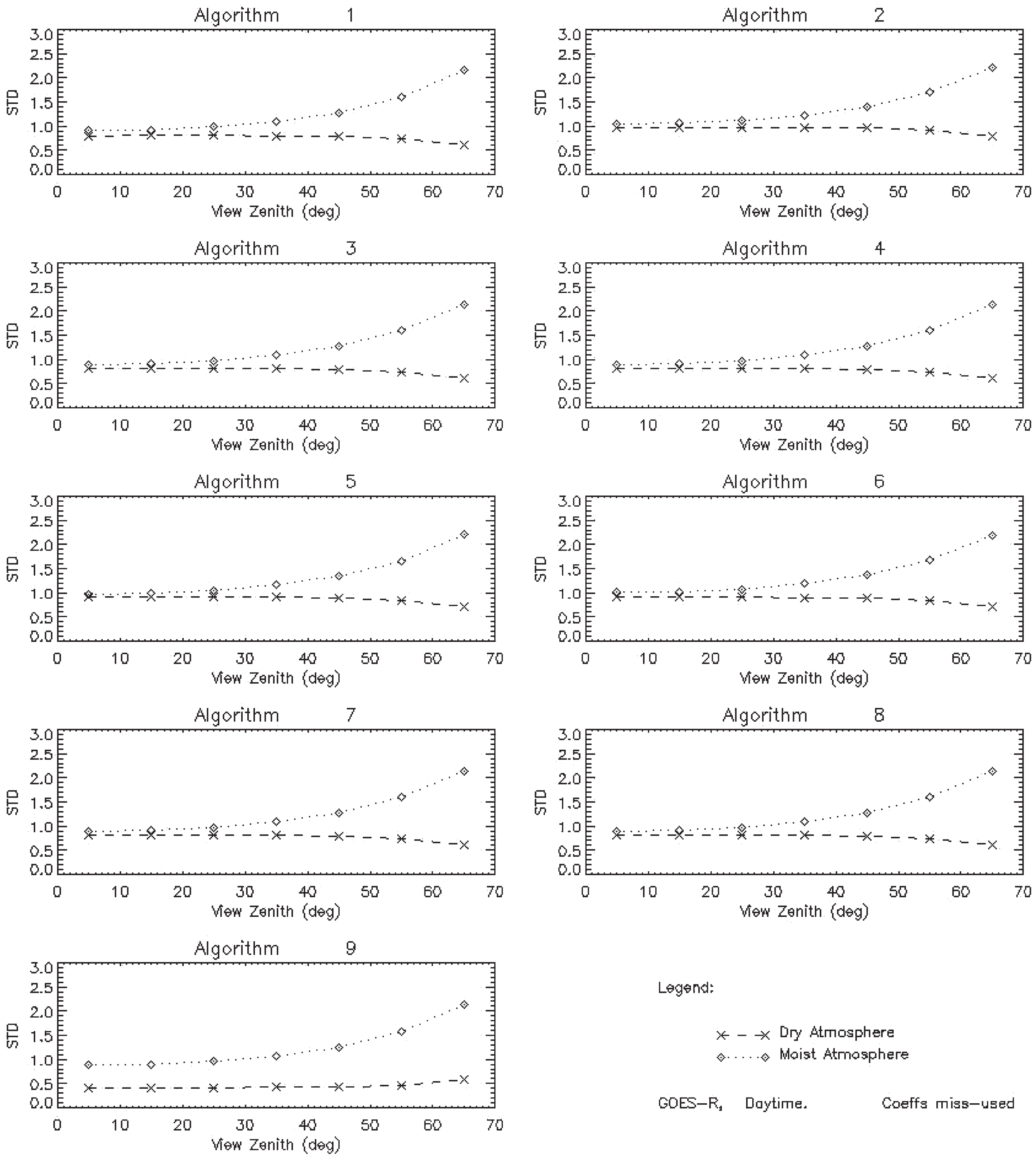

Fig. 7. STD errors when algorithm coefficients are misused (daytime cases). The dashed lines (marked as Dry Atmosphere) represent the errors when the coefficients derived for moist atmosphere are applied for the dry atmospheric LST retrieval; while the dotted lines (marked as Moist Atmosphere) represent the errors when the coefficients derived for dry atmosphere are applied for the moist atmospheric LST retrieval.

B. Algorithm Sensitivity

Emissivity sensitivities of the algorithms were estimated using (1) and are shown in Fig. 6, for the daytime cases. For illustration purposes, we assumed that 1) the mean emissivity (ε) and emissivity difference ($\Delta\varepsilon$) are 0.97 and 0.005, respectively, and 2) the brightness temperatures are 295 K and 294 K for channels 14 and 15 of the ABI sensor, respectively. Results show that the LST uncertainty (δT) increases approximately linearly, and that uncertainty can be significant (up to 3 K) for fairly small uncertainty in emissivity. Thus, the algorithms are very sensitive to the emissivity error. Similar sensitivity results were observed for the nighttime cases and, therefore, are not shown here. Note, however, that the predicted LST uncertainty calculated using (1) represents an extreme situation where all of the emissivity errors worsen the LST retrieval (i.e., the errors always compound rather than cancel each other). In practice, the final LST error may be significantly smaller, since emissivity errors at each channel may cancel each other and the temperature errors δT_1 and δT_2 may cancel each other.

In a relative sense, the sensitivity is lowest for algorithm 6, followed by algorithm 2. This is because, in algorithms 2 and 6, the emissivity difference $(\Delta\varepsilon)$ is not used, and the uncertainty of $\Delta\varepsilon$ can be double that of the mean emissivity. This implies that, to reduce the LST algorithm sensitivity to the emissivity error, the emissivity difference should not be included in the algorithm formulation. Note that emissivity sensitivity for the dry atmosphere is higher than that for the moist atmosphere since the LST algorithms for dry atmospheres are less affected by the atmospheric absorption and, therefore, are more accurate (Table IV).

The water vapor sensitivity of the algorithms is analyzed for daytime and nighttime cases. Fig. 7 shows the daytime cases as an example. In these cases, the STD is calculated separately in each 10° range of view zenith angle from 0° to 70°. Note that, for all algorithms, the algorithm coefficients derived for dry atmospheric conditions are more sensitive if they are incorrectly used for the moist atmospheric conditions. This is particularly true for the nighttime cases since they are moister than the daytime cases. Furthermore, for the moist atmospheric condition cases (the dotted lines), such water vapor sensitivity increases when the satellite zenith angle increases. This is also because the atmosphere is getting moister when the total column water vapor along the view path increases with the increase of satellite zenith angle. For the dry atmospheric condition cases (the dashed lines), the STD is significantly increased (comparing to the values in Table IV), but it does not increase with the view zenith angle. In fact, the STD of the LST errors decreased (and is approaching the values of the moist atmospheric cases in Table IV) when the zenith angle increases. This implies that, even for the dry atmospheric conditions, the coefficient set for the moist atmospheric condition may be applicable when the satellite zenith angle is large.

Finally, the algorithm STD distributions with satellite zenith angle are shown for the daytime cases in Fig. 8. It indicates that, for the moist atmospheric conditions, the STD is getting significantly worse when the zenith angle is larger than 45°. For dry atmospheric conditions, the increase in STD is insignificant. Similar trends were observed for the nighttime cases.

Overall, similar water sensitivity was found in all the algorithms, while algorithms 2 and 6 had significantly smaller emissivity sensitivity than the other algorithms. Because simplicity is an advantage in operational procedures, algorithm 6 was chosen for further evaluation.

C. Evaluation Using SURFRAD and GOES-8 Data

The cloud filtered match-up data pairs of the SURFRAD ground LST and the GOES-8 satellite LST are compared with different scenarios. First, Fig. 9 shows scatter plots of the GOES LSTs (x-axis) versus the SURFRAD LSTs (y-axis) for all match-up pairs; the six panels in the figure represent the six SURFRAD sites. The root mean square (RMS) difference of the SURFRAD LSTs and the GOES LSTs is smallest (1.39 K) at Goodwin Creek and largest (2.52 K) at Desert Rock. Interestingly, the two sites also provide the smallest (0.18 K at Goodwin Creek) and the largest (−1.10 K at Desert Rock) bias of the two LST measurements. The RMS and the bias over all sites are 2.15 K and −0.43 K, respectively. The LST range in this comparison was from 250 K to 330 K, with a total of 11 761 measurement pairs.

The comparison was also performed separately on the daytime and nighttime data and under dry and moist atmospheric conditions, respectively. Results are listed in Table V. For the daytime results in Table V, the smallest RMS (1.44 K) is observed at site 3 (Goodwin Creek), while the largest RMS (2.47 K) is observed at site 6 (Desert Rock). The overall RMS and bias over the six sites are 2.12 K and 0.15 K, respectively. For the nighttime results, the smallest RMS (1.36 K) is observed at Goodwin Creek, while the largest RMS (2.56 K) is observed at Desert Rock. The overall RMS and bias over the six sites are 2.09 K and −0.65 K, respectively.

For the results of dry atmospheric conditions in Table V, the smallest RMS (1.37 K) error was observed at Goodwin Creek, while the largest RMS (2.51 K) error was observed at Desert Rock. Desert Rock may act like a moister site than it is, because it is always viewed from GOES-8 through a long atmospheric path length (with satellite zenith angle 60.15°). The overall RMS and bias over the six sites are 2.17 K and −0.42 K, respectively. For the results of moist atmospheric conditions, the smallest RMS and bias (1.44 K and 0.03 K, respectively) errors were observed at Boulder, while the largest RMS (2.74 K) was observed at Desert Rock and the largest bias (−1.46 K) was observed at site 2 (Bondeville). The overall RMS and bias over the six sites were 1.98 K and −0.49 K, respectively.

Interestingly, the Desert Rock site consistently showed the worst validation results while the Goodwin Creek site showed the best results. The results over all six sites under different atmospheric conditions (RMS of 2.15 K and bias of −0.43 K) meet the GOES-R MRD requirement. As stated earlier, some of this systematic performance difference may be related to the degree of homogeneity over particular sites. The comparison of the point-scale SURFRAD values with GOES-8 pixels inevitably includes large uncertainties due to this scale mismatch.

V. Discussion

We note that all algorithms listed in Table I give similar retrieval accuracy. This primarily indicates the accuracy limitation of the current SW technique. The accuracy difference between the moist and dry atmospheric conditions implies that water vapor contamination is a major concern for the GOES-R LST retrieval. The largest errors are expected with SW algorithms when the atmosphere is moist, and the satellite zenith angle is larger than 45°. The accuracy of the retrieval under dry atmospheric conditions is significantly better than that under

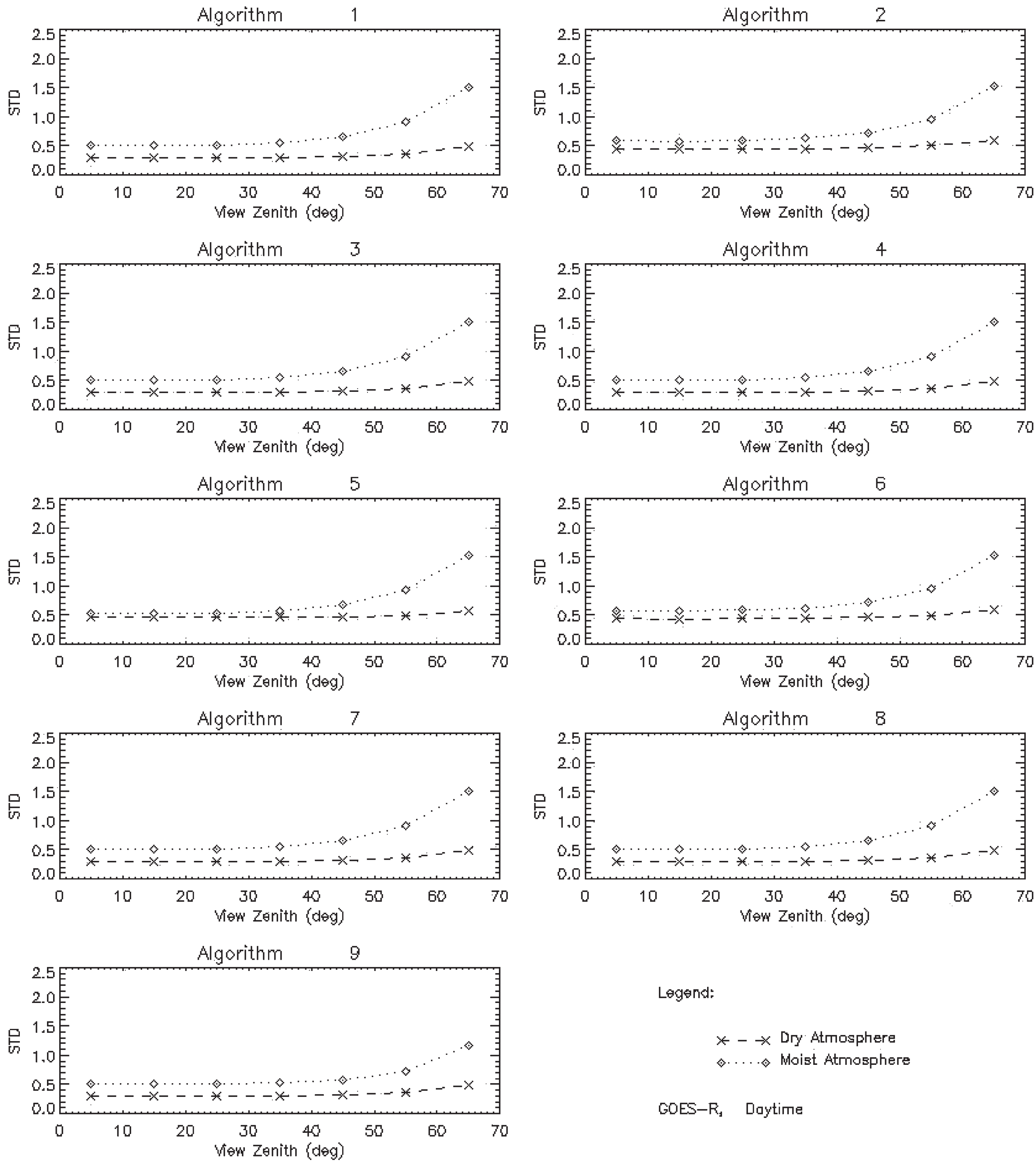

Fig. 8. Daytime algorithm STD errors in different satellite view zenith angles.

moist atmospheric conditions. Similar results were observed in [14].

Emissivity sensitivity is a more serious problem. First, compared to water surface, thermal IR emissivity for most land surface types varies considerably from unity. This is because topographical and vegetation structural variability is complicated, and satellite-sensed brightness temperatures over a given target can differ significantly from one sun-view geometry to another. Moreover, spatial heterogeneity over land is very large compared to oceans, and a retrieved LST represents a complex integration of the observed ensemble within a pixel. Finally, spatial and temporal variation of atmosphere over land is almost always greater than that over oceans.

More importantly, the emissivity effect is coupled with the atmospheric absorption effect in the radiative transfer process; while the atmospheric absorption effect is linearized in the SW

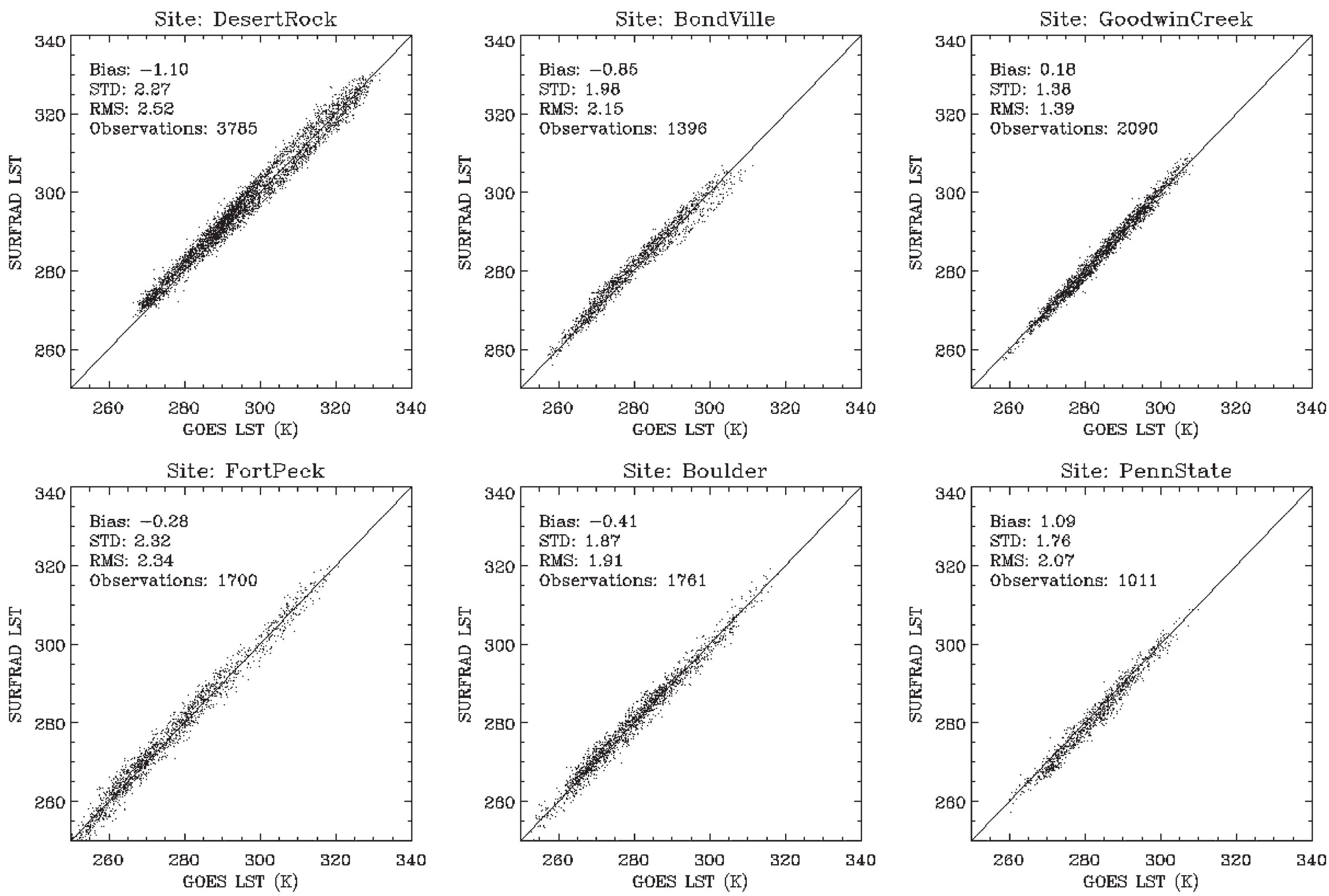

Fig. 9. Scatter plot comparison of the GOES LST and the SURFRAD LST for all the match-up data in 2001, within six SURFRAD sites.

TABLE V

COMPARISON RESULTS (KELVINS) OF THE LSTS RETRIEVED FROM THE GOES-8 IMAGER AND THE SURFRAD GROUND MEASUREMENTS. THE BIAS IS MEASURED AS THE SATELLITE LST MINUS THE SUFRAD LST

	Site 1			Site 2			Site 3			Site 4			Site 5			Site 6		
	Bias	STD	RMS	Bias	STD	RMS	Bias	STD	RMS	Bias	STD	RMS	Bias	STD	RMS	Bias	STD	RMS
Day	0.27	1.57	1.59	0.56	2.15	2.22	-0.17	1.43	1.44	0.43	2.11	2.15	0.25	1.94	1.96	0.03	2.47	2.47
Night	1.56	1.70	2.30	-0.25	1.34	1.37	0.38	1.31	1.36	-0.71	2.34	2.45	-0.82	1.69	1.88	-2.09	1.48	2.56
Dry	1.15	1.75	2.09	-0.77	2.01	2.15	0.28	1.34	1.37	-0.18	2.32	2.33	-0.42	1.88	1.92	-1.13	2.24	2.51
Moist	0.58	1.79	1.89	-1.46	1.59	2.16	-0.24	1.45	1.47	-1.32	2.00	2.40	0.03	1.44	1.44	-0.29	2.73	2.74
Total	1.09	1.76	2.07	-0.85	1.98	2.15	0.18	1.38	1.39	-0.28	2.32	2.34	-0.41	1.87	1.91	-1.10	2.27	2.52

technique [10], [38], the emissivity effect cannot be similarly linearized. A tradeoff in current SW applications occurs since emissivity information improves retrieval accuracy, but inaccurate emissivity information may induce significant error. It is worth pointing out that the same conflict also occurs to those SW LST algorithms, e.g., the LST algorithm developed for the NPOESS Preparatory Project VIIRS sensors [29], which stratify the algorithm coefficients for different land surface types instead of using the emissivity information explicitly in the algorithm. For such algorithms, the emissivity uncertainty of a certain surface type may also induce significant LST retrieval error.

Our results demonstrate that, although using both the mean emissivity and the emissivity difference of the two thermal channels provide the best retrieval accuracy, such algorithms are too sensitive to the emissivity uncertainty and should not be used in operational practice. As a compromise, we recommend algorithm 6, which only requires the mean emissivity information, as the Day 1 algorithm for generating the GOES-R LST product.

Our evaluation results from the SURFRAD data indicate that the accuracy of the derived LST algorithm meets the GOES-R MRD requirement (less than 2.5 K). In a sitewise analysis, however, for some sites under some atmospheric conditions, the accuracies do not meet the requirement (Table V). In particular, the data from Desert Rock (site 6) cannot meet the requirement for any atmospheric condition. The errors likely occur from several sources. First, emissivity uncertainty is significant since emissivity was estimated from the surface-type-emissivity mapping. Note that the emissivity sensitivity of the satellite LST retrieval is different from the emissivity sensitivity of the SURFRAD LST estimation using (5) and (6); the mean spectral emissivity is required in (6) while the spectral emissivity is applied in the satellite LST retrieval. We assume that the effect of the emissivity uncertainty difference is large for the Desert Rock site case. In contrast, the data from Goodwin Creek (site 3) provided consistently good results, indicating that emissivity uncertainty for the site is less significant. Goodwin Creek may be a more uniform site (mostly forest) than the rest.

Second, the static emissivity information used here, both for the satellite LST retrieval and the SURFRAD LST estimation, may introduce errors. Land surface emissivity typically varies along with seasonal vegetation growth and senescence and even diurnal land surface moisture variation. Although few dynamic emissivity maps currently exist and some are in development [37], we recommend that dynamic emissivity information be used for the GOES-R LST retrieval when available.

In addition, angularly anisotropy in surface emission may have significant impacts in the LST ground evaluation process. Note that the SURFRAD LST estimation using (5) and (6) is based on a Lambertian assumption. It has been reported that the "effective" surface emissivity for a satellite pixel varies with view zenith angle due to the surface vegetation–soil structure [39]–[41]. Such emissivity angular anisotropy may be significant in the LST retrieval. Vinnikov *et al.* [42] reported that LSTs observed from GOES-East and GOES-West may be significantly different due to the view geometry differences alone, and such LST differences vary diurnally and seasonally.

Finally, cloud contamination is still a difficulty in our evaluation process even though we have applied a complicated manual filtering process. Further improvement is possible as reported in the study of Vinnikov *et al.* [42].

VI. Concluding Remarks

We have identified an LST retrieval algorithm for the GOES-R mission that meets the required accuracy (< 2.3 K). It was determined from nine candidate SW LST algorithms using a comprehensive simulation database generated from the MODTRAN radiative transfer processing tool. The algorithm is consistent with the one recommended by Yu *et al.* [14] for generating long term LST records from polar-orbiting satellite sensors. It applies prescribed surface emissivity information for specifying land surface types, view zenith angle for the radiative transfer path correction, and split channel signals for atmospheric correction. The algorithm was evaluated using one year of ground measurements and GOES-8 satellite data.

Further studies are necessary to improve the algorithm. First, due to the algorithm sensitivity, emissivity uncertainty is still a main concern in the algorithm development. This is true not only for the LST retrieval accuracy but also for a validation process using systematically collected ground measurements such as those from the SURFRAD network. Obtaining high-quality land surface emissivity information is crucial for a highly accurate satellite LST product.

Water vapor absorption is also an important concern, particularly when the view zenith angle is large or the atmosphere is very moist. Although the SW technique corrects the water vapor absorption using brightness temperature differences between two adjacent thermal infrared channels, a better water vapor correction method is desirable for LST retrieval under moist atmospheres.

Finally, a comprehensive and credible ground validation method is necessary for the GOES-R program. In preparing a match-up satellite and ground measurement data set, there are basically three difficulties: 1) high-quality cloud filtering method; 2) accurate ground LST measurement; and 3) pixel-to-point analysis. Improvements are needed in each area if we are to confidently state and assess trends in the operational product uncertainties.

Acknowledgment

This study was supported through the NOAA GOES-R AWG. The authors would like to thank Dr. F. Weng and Dr. T. Zhu of the GOES-R AWG Proxy Data Team for providing the GOES-8 data and Dr. J. Augustine of the SURFRAD program for providing support in using the SURFRAD data. The manuscript contents are solely the opinions of the authors and do not constitute a statement of policy, decision, or position on behalf of NOAA or the U.S. Government.

References

[1] J. M. Norman and F. Becker, "Terminology in thermal infrared remote sensing of natural surfaces," *Remote Sens. Rev.*, vol. 12, pp. 159–173, 1995.

[2] Z.-L. Li and F. Becker, "Feasibility of land surface temperature and emissivity determination from AVHRR data," *Remote Sens. Environ.*, vol. 43, no. 1, pp. 67–85, Jan. 1993.

[3] D. Jones, "The geospatial technologies in your world," *EOM*, vol. 13, no. 5, Aug./Sep. 2004. [Online]. Available: http://www.eomonline.com/Common/Archives/2004augsep/04augsep_GOES-R.html

[4] *History of GOES: GOES-1 through GOES-7*. [Online]. Available: http://ww2010.atmos.uiuc.edu/(Gh)/guides/rs/sat/goes/oldg.rxml

[5] D. Sun and R. Pinker, "Estimation of land surface temperature from a Geostationary Operational Environmental Satellite (GOES-8)," *J. Geophys. Res.*, vol. 108, no. D11, p. 4326, 2003.

[6] D. Sun and R. Pinker, "Case study of soil moisture effect on land surface temperature retrieval," *IEEE Geosci. Remote Sens. Lett.*, vol. 1, no. 2, pp. 127–130, Apr. 2004.

[7] C. M. Hayden, "GOES-VAS simultaneous temperature-moisture retrieval algorithm," *J. Appl. Meteorol.*, vol. 27, no. 6, pp. 705–733, Jun. 1988.

[8] C. M. Hayden, G. S. Wade, and T. J. Schmit, "Derived product imagery from GOES-8," *J. Appl. Meteorol.*, vol. 35, no. 2, pp. 153–162, Feb. 1996.

[9] T. J. Schmit, W. Paul Menzel, J. Gurka, and M. Gunshor, "The ABI on GOES-R," in *Proc. 3rd Annu. Symp. Future National Operational Environ. Satell. Syst.*, San Antonio, TX, Jan. 16, 2007.

[10] L. M. McMillin and D. S. Crosby, "Theory and validation of the multiple window sea surface temperature technique," *J. Geophys. Res.*, vol. 89, no. C3, pp. 3655–3661, 1984.

[11] E. P. McClain, W. G. Pichel, and C. C. Walton, "Comparative performance of AVHRR-based multichannel sea surface temperatures," *J. Geophys. Res.*, vol. 90, no. C14, pp. 11 587–11 601, Nov. 1985.

[12] C. C. Walton, W. G. Pichel, J. F. Sapper, and D. A. May, "The development and operational application of nonlinear algorithms for the measurement of sea surface temperatures with the NOAA polar-orbiting environmental satellites," *J. Geophys. Res.*, vol. 103, no. C12, pp. 27 999–28 012, 1998.

[13] National Research Council, *Review of NOAA's Plan for the Scientific Stewardship Program*, 2005, Washington, DC: Nat. Academies Press.

[14] Y. Yu, J. P. Privette, and A. C. Pinheiro, "Evaluation of split-window land surface temperature algorithms for generating climate data records," *IEEE Trans. Geosci. Remote Sens.*, vol. 46, no. 1, pp. 179–192, Jan. 2008.

[15] J. C. Jimenez-Munoz and J. A. Sobrino, "Feasibility of retrieving land-surface temperature from ASTER TIR bands using two-channel algorithms: A case study of agricultural areas," *IEEE Geosci. Remote Sens. Lett.*, vol. 4, no. 1, pp. 60–64, Jan. 2007.

[16] K. Mao, J. Shi, H. Tang, Z.-L. Li, X. Wang, and K. Chen, "A neural network technique for separating land surface emissivity and temperature from ASTER imagery," *IEEE Trans. Geosci. Remote Sens.*, vol. 46, no. 1, pp. 1–9, Jan. 2008.

[17] L. M. McMillin, "Estimation of sea surface temperatures from two infrared window measurements with different absorption," *J. Geophys. Res.*, vol. 80, no. C36, pp. 5113–5117, 1975.
[18] GOES-R Program Office, *GOES-R Series Mission Requirements Document (MRD)*, 2007. P417-R-MRD-0070.
[19] Z. Wan and J. Dozier, "A generalized split-window algorithm for retrieving land-surface temperature from space," *IEEE Trans. Geosci. Remote Sens.*, vol. 34, no. 4, pp. 892–905, Jul. 1996.
[20] F. Becker and Z. L. Li, "Towards a local split window method over land surfaces," *Int. J. Remote Sens.*, vol. 11, no. 3, pp. 369–393, 1990.
[21] A. J. Prata and C. M. R. Platt, "Land surface temperature measurements from the AVHRR," in *Proc. 5th AVHRR Data Users Conf.*, Tromso, Norway, Jun. 25–28, 1991, pp. 438–443. EUM P09.
[22] V. Caselles, C. Coll, and E. Valor, "Land surface temperature determination in the whole Hapex Sahell area from AVHRR data," *Int. J. Remote Sens.*, vol. 18, no. 5, pp. 1009–1027, 1997.
[23] A. Vidal, "Atmospheric and emissivity correction of land surface temperature measured from satellite using ground measurements or satellite data," *Int. J. Remote Sens.*, vol. 12, no. 12, pp. 2449–2460, 1991.
[24] J. C. Price, "Land surface temperature measurements from the split window channels of the NOAA-7/AVHRR," *J. Geophys. Res.*, vol. 89, pp. 7231–7237, 1984.
[25] C. Ulivieri and G. Cannizzaro, "Land surface temperature retrievals from satellite measurements," *Acta Astronaut.*, vol. 12, no. 12, pp. 985–997, 1985.
[26] J. A. Sobrino, Z. L. Li, M. P. Stoll, and F. Becker, "Improvements in the split-window technique for land surface temperature determination," *IEEE Trans. Geosci. Remote Sens.*, vol. 32, no. 2, pp. 243–253, Mar. 1994.
[27] C. Ulivieri, M. M. Castronouvo, R. Francioni, and A. Cardillo, "A SW algorithm for estimating land surface temperature from satellites," *Adv. Space Res.*, vol. 14, no. 3, pp. 59–65, 1992.
[28] C. Coll, C. Caselles, J. A. Sobrino, and E. Valor, "On the atmospheric dependence of the split-window equation for land surface temperature," *Int. J. Remote Sens.*, vol. 15, no. 1, pp. 1915–1932, Jan. 1994.
[29] R. J. Sikorski, P. S. Kealy, and W. J. Emery, *Land Surface Temperature Visible/Infrared Image Radiometer Suite Algorithm Theoretical Basis Document*, 2002, Raytheon Systems Company. Version 5. [Online]. Available: http://npoesslib.ipo.noaa.gov/atbd/viirs/
[30] A. C. Pinheiro, R. Mahoney, L. Privette, and C. J. Tucker, "Development of a daily long term record of NOAA-14 AVHRR land surface temperature over Africa," *Remote Sens. Environ.*, vol. 103, no. 2, pp. 153–164, 2006.
[31] Y. Yu, J. L. Privette, and A. C. Pinheiro, "Analysis of the NPOESS VIIRS land surface temperature algorithm using MODIS data," *IEEE Trans. Geosci. Remote Sens.*, vol. 43, no. 10, pp. 2340–2350, Oct. 2005.
[32] A. Berk, G. P. Anderson, P. K. Acharya, J. H. Chetwynd, M. L. Hoke, L. S. Bernstein, E. P. Shettle, M. W. Matthew, and S. M. Alder-Golden, *MODTRAN4 Version 2 User's Manual*. Lexington, MA: Space Vehicles Directorate, Hanscom AFB, Apr. 2000.
[33] W. C. Snyder, Z. Wan, and Y. Z. Feng, "Classification-based emissivity for land surface temperature measurement from space," *Int. J. Remote Sens.*, vol. 19, no. 14, pp. 2753–2774, 1998.
[34] J. A. Augustine, J. J. DeLuisi, and C. N. Long, "SURFRAD—A national surface radiation budget network for atmospheric research," *Bull. Amer. Meteorol. Soc.*, vol. 81, no. 10, pp. 2341–2357, Oct. 2000.
[35] J. A. Augustine, G. B. Hodges, C. R. Cornwall, J. J. Michalsky, and C. I. Medina, "An update on SURFRAD—The GCOS surface radiation budget network for the continental United States," *J. Atmos. Oceanic Technol.*, vol. 22, no. 10, pp. 1460–1472, Oct. 2005.
[36] M. Hansen and B. Reed, "A comparison of the IGBP DISCover and University of Maryland 1 km global land cover products," *Int. J. Remote Sens.*, vol. 21, no. 6/7, pp. 1365–1373, 2000.
[37] K. Wang, Z. Wan, P. Wang, M. Sparrow, J. Liu, X. Zhou, and S. Haginoya, "Estimation of surface long wave radiation and broadband emissivity using Moderate Resolution Imaging Spectroradiometer (MODIS) land surface temperature/emissivity products," *J. Geophys. Res.*, vol. 110, p. D11 109, 2005.
[38] Y. Yu and I. J. Barton, "A non-regression-coefficients method of sea surface temperature retrieval from space," *Int. J. Remote Sens.*, vol. 15, no. 6, pp. 1189–1206, 1994.
[39] A. C. Pinheiro, J. L. Privette, J. Pedelty, and J. Bates, "Satellite retrievals of land surface temperature: Challenges and opportunities, 20th conference on climate variability and change," in *Proc. 88th AMS Annu. Meeting*, New Orleans, LA, 2008.
[40] A. C. Pinheiro, J. L. Privette, R. Mahoney, and C. J. Tucker, "Directional biases in a 5-year Daily AVHRR land surface temperature product over Africa," *IEEE Trans. Geosci. Remote Sens.*, vol. 42, no. 9, pp. 1941–1954, Sep. 2004.
[41] Y. Yu, A. C. Pinheiro, and J. L. Privette, *Correcting Land Surface Temperature Measurements for Directional Emissivity Over 3-D Structured Vegetation*. San Diego, CA: SPIE, Jul. 2006.
[42] K. Y. Vinnikov, Y. Yu, M. K. Rama Varma Raja, J. D. Tarpley, and M. D. Goldberg, "Seasonal, diurnal, and weather related variations of clear sky land surface temperature: A statistical assessment," in *Proc. AMS Annu. Meeting*, New Orleans, LA, Jan. 2008. P1.56.

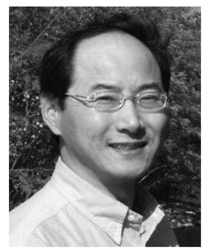

Yunyue Yu received the B.Sc. degree in physics from the Ocean University of Qingdao (OUQ), Qingdao, China, in 1982, the M.Sc. degree equivalent in advanced physics from the Peking University, Beijing, China, in 1986, and the Ph.D. degree in aerospace engineering sciences from the University of Colorado (CU), Boulder, in 1996.

During his tenure with OUQ (1982–1993), he was a Lecturer and an Associate Professor and held leadership roles in multiple international corporation projects. From 1987 to 1992, he was a Visiting Scientist at the University of Dundee, Dundee, U.K., the Division of Atmospheric Research, Australian Commonwealth Scientific and Industrial Research Organization, and the Colorado Center for Astrodynamics Research, CU. In 1996, he was with the Earth Observation System Satellites program through Raytheon ITSS and George Mason University and with NASA Goddard Space Flight Center. He has accomplished a variety of projects in ocean and land surface remote sensing and applications. Currently, he is a Physical Scientist with the National Environmental Satellite, Data, and Information Service Center for Satellite Applications and Research, National Oceanic and Atmospheric Administration, Camp Springs, MD, the Chairman of the land surface algorithms working group of the GOES-R satellite mission, and a member of the National Polar-orbiting Operational Environmental Satellite System Visible/Infrared Imager Radiometer Suite Operational Algorithm Team.

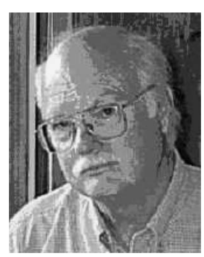

Dan Tarpley received the B.S. degree in physics from Texas Tech University and the Ph.D. degree in atmospheric physics from the University of Colorado.

He is a Consultant with the National Environmental Satellite, Data, and Information Service Center for Satellite Applications and Research, National Oceanic and Atmospheric Administration, working primarily on the GOES-R algorithm development. His interests include the development and use of remotely sensed snow cover, vegetation conditions, land surface temperature, surface radiation budget, and precipitation products for validation and boundary conditions in numerical weather prediction models.

Jeffrey L. Privette received the B.S. degrees from the University of Michigan, Ann Arbor, and The College of Wooster, Wooster, OH, and the M.S. and Ph.D. degrees from the University of Colorado, Boulder, in 1994.

During his tenure with NASA (1996–2006), he held leadership positions in SAFARI 2000, the Moderate Resolution Imaging Spectroradiometer (MODIS) Land Validation Program, and the Committee on Earth Observation Satellites Working Group for Calibration and Validation. He was NASA's Deputy Project Scientist for the National Polar-orbiting Operational Environmental Satellite System (NPOESS) Preparatory Project from 2002 to 2006. Since 2006, he has been with the National Environmental Satellite, Data, and Information Service National Climatic Data Center, National Oceanic and Atmospheric Administration (NOAA), Asheville, NC, serving as the Project Manager of Scientific Data Stewardship (SDS). The SDS Project coordinates and executes NOAA's activities in climate data records. He is also the Land Validation Lead and a Visible/Infrared Imager Radiometer Suite Operational Algorithm Team member for the NPOESS program. His research has focused on the retrieval and validation of land biophysical parameters from wide field-of-view imagers (e.g., Advanced Very High Resolution Radiometer and MODIS), with a special emphasis on directional effects.

Mitchell D. Goldberg is the Chief of the Satellite Meteorology and Climatology Division, National Environmental Satellite, Data, and Information Service (NESDIS) Center for Satellite Applications and Research, National Oceanic and Atmospheric Administration (NOAA), Camp Springs, MD, and the Program Manager for the GOES-R Algorithm Working Group. He has extensive experience in the development and improvement of algorithms for deriving atmospheric temperature and moisture profiles from satellite observations. In 1990, he was with the NESDIS Office of Research and Applications. He is a member of the competitively awarded NASA Atmospheric Infrared Sounder science team and the European Organization for the Exploitation of Meteorological Satellites Infrared Atmospheric Sounding Interferometer Science Working Group. He contributes to both teams by developing and validating scientific algorithms for deriving geophysical parameters from space-based hyperspectral infrared observations and also oversees the development of processing systems for data distribution. He also serves on the Integrated Program Office National Polar-orbiting Operational Environmental Satellite System (NPOESS) Sounding Operational Algorithm Team, which is an advisory board for the hyperspectral NPOESS Cross-track InfraRed Sounder. He is also a member of the NOAA Climate Board and the World Meteorological Organization Atmospheric Observations Panel for Climate. In 2002, he was promoted to Chief of the Climate Research and Applications Division, which was reorganized into the Satellite Meteorology and Climatology Division. The division, consisting of nearly 40 federal employees and supported by more than 60 contractors and visiting scientists, applies remote sensing science to monitoring and describing the Earth/atmosphere system, develops and demonstrates new applications of satellite data and product processing systems, provides calibration of satellite instruments, validates satellite products, conducts training, and transfers technology to operations.

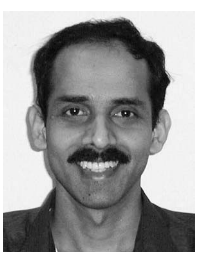

M. K. Rama Varma Raja received the B.Sc. degree in physics from the University of Calicut, Kerala, India, the M.Tech. degree in atmospheric physics from the University of Pune, Pune, India, the M.Sc. degree in meteorology from the Andhra University, Visakhapatnam, India, and the Ph.D. degree from the University of Pune, in 2000.

He was with the Office of Research and Applications, National Environmental Satellite, Data, and Information Service (NESDIS), National Oceanic and Atmospheric Administration (NOAA) in June 2000 as an Associate Fellow of Cooperative Institute for Research in Atmosphere (Colorado Sate University). Since May 2003, he has been a Physical Scientist with I. M. Systems Group, Inc., Camp Springs, MD, working on NOAA/NESDIS/Center for Satellite Applications and Research projects. His research has focused on validating the retrieval products such as winds from Doppler lidars, water vapor and trace gases from infrared sounders, and land surface temperature from IR radiometers. He has extensive analysis experience in global-positioning-system-based water vapor data and also in the analysis of data from mesosphere–stratosphere–troposphere radars. He has many peer reviewed scientific publications to his credit and recently coauthored a Journal of Geophysical Research (2007) paper which won the NOAA Office of Applications and Research 2008 Outstanding Scientific Paper Award.

Konstantin Y. Vinnikov received the Ph.D. degree from the Voeikov Main Geophysical Observatory, St. Petersburg, Russia, in 1966 and the D.Sc. degree from the Higher Certifying Commission of the Council of Ministers of the former USSR in 1983.

He is currently a Senior Research Scientist with the Department of Atmospheric and Oceanic Science, University of Maryland, College Park. His research interests include climate change and remote sensing.

Hui Xu received the B.Sc. degree in geography from Beijing University, Beijing, China, the M.Sc. degree in land and water management from Cranfield Institute of Technology, Cranfield, U.K., and the Ph.D. degree in geography from the University of Edinburgh, Edinburgh, U.K.

She worked in remote sensing data application, research and product development, as well as integration of remote sensing and geographic information systems (GIS). She was a project scientist for snow mapping and snow depth monitoring with the University of Bristol. Her work at Nottingham University on monitoring the leaf area of sugar beet using ERS-1 SAR data contributed to a yield prediction project for the British Sugar. She taught remote sensing and GIS courses as an Assistant Professor with Frostburg State University, MD, before joining I. M. Systems Group, Inc., Camp Springs, MD, in 2001. Since then, she has worked with the National Oceanic and Atmospheric Administration (NOAA) Science Center on various projects, including rehosting, documentation, and validation of the Automatic Snow Mapping System, on-orbit verification and intersatellite calibration of NOAA polar-orbiting radiometers, and her current participation in the GOES-R algorithm development and testing of normalized difference vegetation index and land surface temperature products in the land application team.